Potential high-T_c superconducting lanthanum and yttrium hydrides at high pressure

Hanyu Liu[a], Ivan I. Naumov[a], Roald Hoffmann[b], N. W. Ashcroft[c], and Russell J. Hemley[d,e,1]

[a]Geophysical Laboratory, Carnegie Institution of Washington, Washington, DC 20015; [b]Department of Chemistry and Chemical Biology, Cornell University, Ithaca, NY 14853; [c]Laboratory of Atomic and Solid State Physics, Cornell University, Ithaca, NY 14853; [d]Department of Civil and Environmental Engineering, The George Washington University, Washington, DC 20052; and [e]School of Applied and Engineering Physics, Cornell University, Ithaca, NY 14853

Contributed by Russell J. Hemley, May 5, 2017 (sent for review March 20, 2017; reviewed by Panchapakesan Ganesh, Jeffrey M. McMahon, and Dimitrios Papaconstantopoulos)

A systematic structure search in the La–H and Y–H systems under pressure reveals some hydrogen-rich structures with intriguing electronic properties. For example, LaH_{10} is found to adopt a sodalite-like face-centered cubic (fcc) structure, stable above 200 GPa, and LaH_8 a *C2/m* space group structure. Phonon calculations indicate both are dynamically stable; electron phonon calculations coupled to Bardeen–Cooper–Schrieffer (BCS) arguments indicate they might be high-T_c superconductors. In particular, the superconducting transition temperature T_c calculated for LaH_{10} is 274–286 K at 210 GPa. Similar calculations for the Y–H system predict stability of the sodalite-like fcc YH_{10} and a T_c above room temperature, reaching 305–326 K at 250 GPa. The study suggests that dense hydrides consisting of these and related hydrogen polyhedral networks may represent new classes of potential very high-temperature superconductors.

high pressure | superconductivity | hydrides | structure search

Extending his original predictions of very high-temperature superconductivity of high-pressure metallic hydrogen (1), Ashcroft later proposed that hydrogen-rich materials containing main group elements might exhibit superconductivity at lower pressures, as the hydrogen in these structures may be considered "chemically precompressed" (2). These proposals, which were based on the Bardeen–Cooper–Schrieffer (BCS) (3) phonon-mediated theory of superconductivity, have motivated many theoretical and experimental efforts in the search for high-temperature superconductivity in hydrides at elevated pressures (4–10). Theory has predicted the stability of a variety of dense hydride structures for which BCS arguments give superconducting transition temperatures, T_cs, that are very high (11–18).

In recent times, compression of hydrogen sulfides has provided a new incentive in hydride superconductivity, one in which theory played an important role. First, theoretical calculations predicted H_2S to have a T_c of ∼80 K at pressures above 100 GPa (19). Compression of H_2S led to the striking discovery of a superconducting material with a T_c of 203 K at 200 GPa (20). Moreover, the critical temperature exhibits a pronounced isotope shift consistent with BCS theory. It was proposed that the superconducting phase is not stoichiometric H_2S but SH_3, with a calculated T_c of 194 K at 200 GPa including anharmonic effects (21, 22). A subsequent experiment (23) suggested that the superconducting phase is cubic SH_3, in agreement with a theoretical study that gave $T_c = 204$ K within the harmonic approximation (24). Compression of another hydride, PH_3, was reported to reach a T_c of ∼100 K at high pressures (25). Subsequent theoretical calculations predicted possible structures and calculated T_cs close to the experimental results (26–28). The experimental picture for these materials remains not entirely clear, and the synthesis of the superconducting phases, which has been reproduced for hydrogen sulfide, is path-dependent (23).

There is great experimental and theoretical interest in searching for related materials with both higher T_c and potentially broader ranges of stability. To date, simple hydrides with the highest predicted superconducting T_cs are MgH_6 (271 K at 300 GPa) (29), CaH_6 (235 K at 150 GPa) (17), and YH_6 (264 K at 120 GPa) (30). In searching for other high-T_c superconducting hydrides, here we investigated theoretically possible high-pressure crystal structures of La–H and Y–H. We predict the existence of new stable hydride phases of these elements, with remarkably high T_cs at attainable pressures. The search for low-energy crystalline structures of La–H was performed using particle swarm optimization methodology implemented in the CALYPSO code (31, 32). This method has been applied successfully to a wide range of crystalline systems ranging from elemental solids to binary and ternary compounds (33–35) and has proven to be a powerful tool for predicting crystal structures at high pressures (36–39). Structure searches were performed in the pressure range of 150–300 GPa using models consisting of 1–4 formula units. In general, the structure search was terminated after the generation of 1,500 structures. Structural optimizations, enthalpies, electronic structures, and phonons were calculated using density-functional theory (DFT). Structure relaxations were performed using DFT using the Perdew–Burke–Ernzerhof (40) generalized gradient approximation. Phonon dispersion and electron–phonon coupling (EPC) calculations were performed with density functional perturbation theory. Ultrasoft pseudopotentials for La and H were used with a kinetic energy cutoff of 80 Ry. A q mesh of $6 \times 6 \times 6$ and k mesh of $24 \times 24 \times 24$ for fcc-LaH_{10} structure in the first Brillouin zone (BZ) was used in the EPC calculations. The superconductivity calculations were performed with the Quantum-ESPRESSO package (17).

Significance

Theoretical predictions and subsequent experimental observations of high-temperature superconductivity in dense hydrogen-rich compounds have reinvigorated the field of superconductivity. A systematic computational study of the hydrides of lanthanum and yttrium over a wide composition range reveals hydrogen-rich structures with intriguing electronic properties under pressure. Electron–phonon coupling calculations predict the existence of new superconducting phases, some exhibiting superconductivity in the range of room temperature. Moreover, the calculated stabilities indicate the materials could be synthesized at pressures that are currently accessible in the laboratory. The results open the prospect for the design, synthesis, and recovery of new high-temperature superconductors with potential practical applications.

Author contributions: H.L. and R.J.H. designed research; H.L., I.I.N., R.H., N.W.A., and R.J.H. analyzed data; and H.L., I.I.N., R.H., N.W.A., and R.J.H. wrote the paper.

Reviewers: P.G., Oak Ridge National Laboratory; J.M.M., Washington State University; and D.P., George Mason University.

The authors declare no conflict of interest.

[1]To whom correspondence should be addressed. Email: rhemley@gwu.edu.

This article contains supporting information online at www.pnas.org/lookup/suppl/doi:10.1073/pnas.1704505114/-/DCSupplemental.

Results

We began with structure searches at ambient pressure for LaH_2. The fcc structure is found to be stable at low pressure, in agreement with experiment. Thinking the high-pressure regime would be most productive for new stoichiometries, we moved directly to 150 and 300 GPa. We first performed structure prediction at 150 and 300 GPa for LaH_x (x = 1–12). LaH_2, LaH_3, LaH_4, LaH_5, LaH_8, and LaH_{10} are found to be stable at 150 GPa (Fig. 1). Note that this figure is plotted with LaH_2 as the lanthanum-rich endpoint, because this composition has the most negative enthalpy/atom at every pressure considered. Fig. 2 shows the computed geometries for the most stable phases we found at each stoichiometry, for n = 2–8. Interestingly, the stable phase predicted for LaH_6 is not sodalite-type but an R-3m structure. The convex hull shows that LaH_6 is not stable from 150 to 300 GPa (Fig. S1); LaH_5 in a P-1 structure is stable from 150 to 200 GPa. LaH_2 adopts a $C2/m$ structure with a H–H distance of 1.53 Å, LaH_3 adopts a $Cmcm$ structure with H–H distance of 1.42 Å, and LaH_8 has a $C2/m$ structure with H–H distance of 1.02 Å (all at 300 GPa).

Most interestingly, we find that LaH_{10} adopts a sodalite-like structure with the La atoms arrayed on an fcc rather than a bcc lattice (Fig. 3). To illustrate the difference between fcc LaH_{10} and previous sodalite-like bcc CaH_6/YH_6 structure, Fig. 3B shows the sodalite-like LaH_6 structure. The fcc-LaH_{10} structure contains [$4^6 6^{12}$] polyhedra which contain hydrogen cubes (Fig. 3 A and C), whereas conventional sodalite is built up of [$4^6 6^8$] polyhedra (Fig. 3 B and D). The H network, made of different atoms, is known in the clathrate and zeolite community as AST (41). The La atoms sit at the 4b Wyckoff position (0, 0, 0), the H atoms at the 32f position (0.12, 0.38, 0.12) and 8c position (0.25, 0.25, 0.75). The shortest H–H distance is 1.1 Å (250 GPa), which is close to H–H distance predicted for atomic metallic hydrogen near 500 GPa (1 Å) (1). In contrast, the H–H distance in sodalite-type CaH_6 is 1.24 Å at 150 GPa.

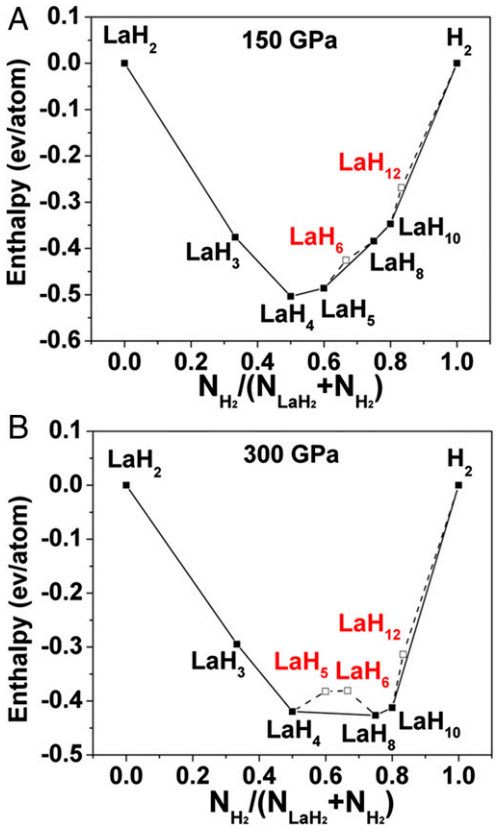

Fig. 1. Formation enthalpy of predicted structures in the La–H system at (A) 150 GPa, (B) 300 GPa. The x axis is the concentration of hydrogen pairs in the stoichiometric compositions considered as described by the generic formula $(H_2)_x(LaH_2)_{1-x}$ ($0 < x < 1$). The enthalpies are shown relative to the ground states of H_2 and LaH_2 at each pressure.

The above structures of LaH_{10} encouraged us to explore the Y–H system at similar pressures (Fig. S2). Previously, YH_3 was predicted to adopt an fcc structure of Y, with atomic H located in the tetrahedral and octahedral interstitial sites. The compound was predicted to be superconducting with a maximum T_c is 40 K near 18 GPa (μ^* = 0.1) (16). Another theoretical study suggested two energetically competing hydrogen-rich polymorphs YH_4 and YH_6 (30). At 120 GPa, both are predicted to be superconductors with maximum T_c of 95 K and 264 K for YH_4 and YH_6, respectively. Our calculations indicate that YH_6 is stable in the sodalite structure up to 300 GPa (Fig. 4 and Fig. S2). As expected, YH_{10} adopts the same structure as LaH_{10} over a range of pressures. We predict that YH_{10} is the energetically stable phase from 250 to 300 GPa, and is dynamically stable down to 220 GPa.

Fig. 5 shows computed YH_n geometries for the most stable phases found at each stoichiometry, for n = 2, 3, 4, 6, 8, and 12. The YH_2 adopts a $P6/mmm$ structure with H–H distances of 1.46 Å at 300 GPa. The YH_3 is stable from 150 to 250 GPa and adopts a $Pnma$ structure with H–H distances of 1.54 Å at 300 GPa (Fig. S2). The YH_4 adopts an $I4/mmm$ structure with H–H distances of 1.37 Å at 300 GPa. It is interesting to see that YH_6 has the same sodalite structure as CaH_6 from 150 to 300 GPa with H–H distances of 1.19 Å at 300 GPa and is stable from 150 to 300 GPa. We found YH_8 is unstable from 150 to 300 GPa with a Cc structure (Fig. S2). The YH_{12} is stable from 50 to 250 GPa and is a $C2/c$ structure with shortest H–H distances of 0.79 Å at 250 GPa.

Before calculating possible superconducting properties we analyze the electronic band structures of the $C2/m$-LaH_8 and fcc-LaH_{10} structures. The band dispersion shows the metallic character of both structures at these pressures (Fig. 6). The fcc LaH_{10} is a good metal with several bands crossing the Fermi level along many directions. This fact manifests itself in a noticeable density of electronic states at the Fermi level: 10.0 states/Ry, which is a factor of 1.4 higher than that previously found in SH_3 (42) at an optimal pressure of 200 GPa (Fig. S3). Remarkably, not only the d electrons of La and s electrons of H contribute to $N(E_f)$ but also f electrons of La; moreover, the latter contribution is dominant. This is due to the fact that external pressure destabilizes La 6s and La 5d orbitals to a greater extent than La 4f: the first two have five and two nodes in their radial wave functions, respectively, whereas the latter has none. This is in sharp contrast with the YH_{10} system, where only the d electrons of Y and s electrons of H are the main contributors to $N(E_f)$. Phonon calculations reveal no imaginary frequencies for LaH_8 and LaH_{10} over a wide pressure range, indicating dynamic stability. Specifically, we find that the structure shown for LaH_{10} is dynamically stable down to 210 GPa. The EPC calculations for different phonon modes indicate that there are no significant contributions in particular directions (Fig. 6 C and D). Note that there are no high-frequency vibrations, consistent with the absence of molecular H_2 entities. The highest frequency for the structure here (2,000 cm^{-1}) can be compared to the 2,600 cm^{-1} calculated for atomic metallic hydrogen in the Cs-IV structure at 500 GPa (43); the lower frequency for the former suggests still weaker H–H interactions in the hydride.

Electron-coupling calculations for LaH_4 give a relatively small λ of 0.43. The estimated T_c is 5–10 K at 300 GPa with the typical choice of the Coulomb potential of μ^* = 0.1–0.13. Using the McMillan equation (44), we calculated T_c using the spectral

PHYSICS

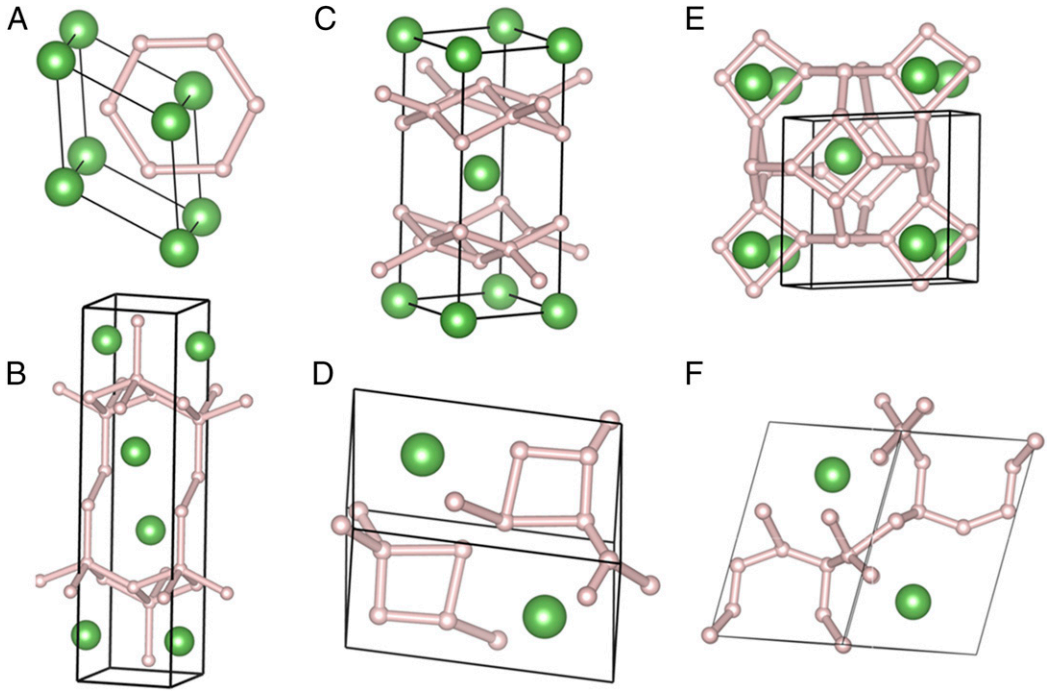

Fig. 2. Predicted lanthanum hydride structures. (*A*) LaH_2, (*B*) LaH_3, (*C*) LaH_4, (*D*) LaH_5, (*E*) LaH_6, and (*F*) LaH_8. Large and small spheres represent La and H atoms.

function [$\alpha^2F(\omega)$], again with $\mu^* = 0.1$–0.13, as previously used in superconductivity calculations for Y (15), La (45, 46), SH_3 (24), CaH_6 (17), YH_6 (30), and other superconductors.

$$T_c = \frac{\omega_{log}}{1.2} exp\left(\frac{-1.04(1+\lambda)}{\lambda - \mu^*(1+0.62\lambda)}\right). \quad [1]$$

Here, λ is the first reciprocal moment of $\alpha^2F(\omega)$,

$$\lambda = 2\int_0^\infty \frac{\alpha^2F(\omega)}{\omega} d\omega \approx \sum_{qj} \lambda_{qj}\omega(\boldsymbol{q}), \quad [2]$$

and $\omega(\boldsymbol{q})$ is the weight of a $\boldsymbol{q}$ (wave vector of crystal vibrations) point in the first BZ. The EPC spectral function $\alpha^2F(\omega)$ is expressed in terms of the phonon linewidth γ_{qj} arising from EPC,

$$\alpha^2F(\omega) = \frac{1}{2\pi N_f} \sum_{qj} \frac{\gamma_{qj}}{\omega_{qj}} \delta(\omega - \omega_{qj})\omega(\boldsymbol{q}). \quad [3]$$

In this equation, N_f is the electronic density of electron states at the Fermi level. The linewidth γ_{qj} of a phonon mode j at wave vector $\boldsymbol{q}$, arising from EPC is given by

$$\gamma_{qj} = 2\pi\omega_{qj} \sum_{nm} \int d^3k/\Omega_{bz} \left|g^j_{kn,k+qm}\right|^2 \times \delta(\xi_{kn} - \xi_F) \times \delta(\xi_{k+qm} - \xi_F), \quad [4]$$

where the sum is over the first BZ, with Ω_{BZ} as the volume of the BZ, and ξ_{kn} are the energies of bands measured with respect to the Fermi ξ_F level at point k. Here, $g^j_{kn,k+qm}$ is the electron–phonon matrix element for scattering from an electron in band n at wave vector k state to band m at wave vector $\boldsymbol{k}+\boldsymbol{q}$ via a phonon with wave vector $\boldsymbol{q}$.

The calculated electron-coupling parameter for LaH_8 at 300 GPa is relatively large (λ = 1.12), and the calculated T_c is 114–131 K,

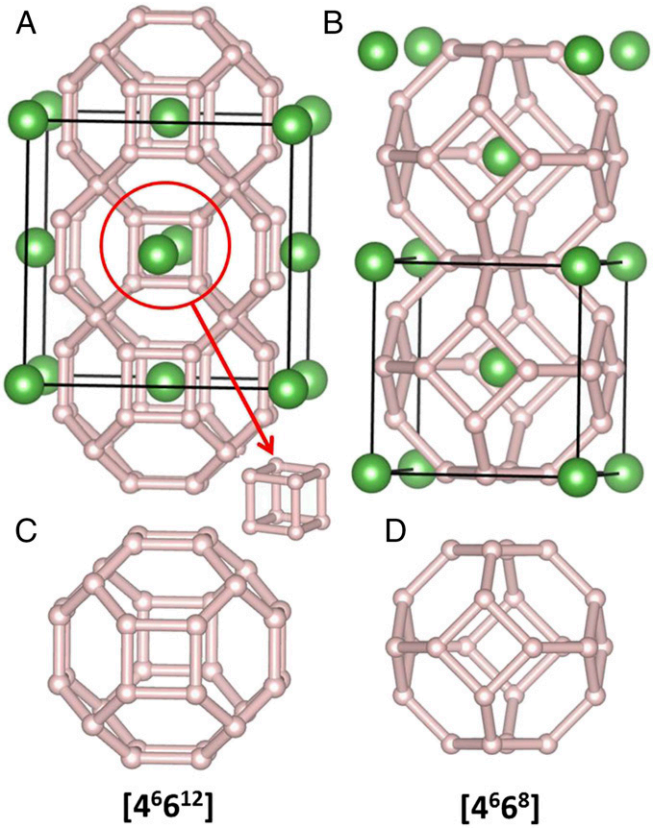

Fig. 3. Crystal structure of sodalite-like LaH_{10} (*A*) and LaH_6 (*B*) at 300 GPa. In the LaH_{10} structure, the red circle highlights the cube hydrogen units. The bottom shows the [4^66^{12}] (*C*) and [4^66^8] (*D*) hydrogen polyhedra in these structures.

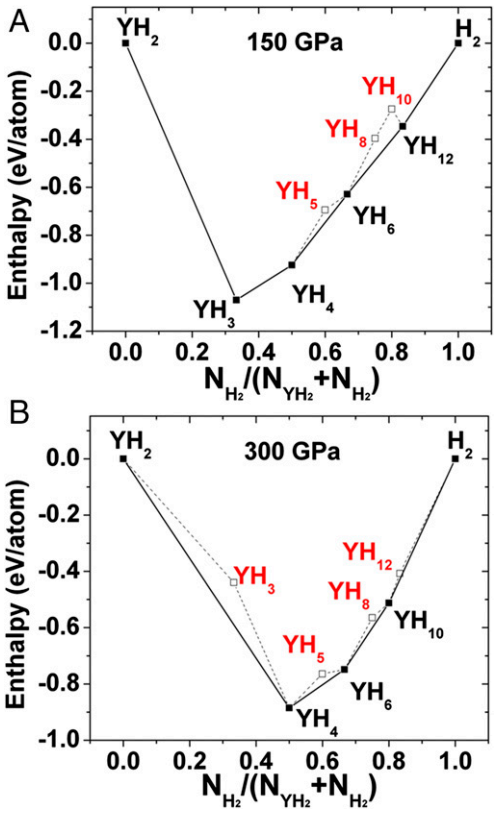

Fig. 4. Formation enthalpy of predicted structures in the Y–H system at (*A*) 150 GPa, (*B*) 300 GPa. The enthalpies are shown relative to the ground states of H_2 and YH_2 at each pressure.

assuming $\mu^* = 0.1$–0.13 (Eq. **1**). That result encouraged us to calculate the T_c of LaH_{10}. Previous theoretical studies also found that sodalite-structured hydrides (e.g., CaH_6 and YH_6) were associated with calculated high-T_c superconductivity. In the LaH_{10} structure, the predicted shortest H–H distance is 1.1 Å (Fig. S4) at these pressures, indicating some H. . .H interactions and no clear distinction between stretching and bending vibrations. As a result, all H vibrations effectively participate in the EPC process, which appears to enhance high superconductivity. The calculated EPC is quite large ($\lambda = 2.2$). T_c was estimated from $\alpha^2F(\omega)$ by numerically solving the Eliashberg equations (17, 30) with $\mu^* = 0.1$–0.13. Coulomb repulsion is taken into account in terms of μ^* scaled to a cutoff frequency. At 250 GPa, the estimated T_c of LaH_{10} is 257–274 K with $\mu^* = 0.1$–0.13. The calculated T_c is found to decrease with increasing pressure (Fig. 7 and Table S1). The predicted T_c for YH_{10} is very high (Fig. 7) using similar EPC calculations. At 250 GPa, the λ is 2.56 and gives a T_c of 305–326 K with $\mu^* = 0.1$–0.13 based on numerically solving the Eliashberg equations. The T_c of YH_{10} increased by ∼30 K relative to YH_6 (30) despite the fact that λ decreases (from 2.93 to 2.56). But, this change is offset by the higher average ω_{log} calculated for YH_{10} compared with YH_6 (1,282 K versus 1,124 K), as a result of the higher hydrogen content in the former. The information of all predicted structures for La–H and Y–H is summarized in Table S2.

Discussion

We now examine the above results, including various assumptions and comparisons with previous studies. Because zero-point energy (ZPE) has been shown to play an important role in determining the stability of hydrogen-rich materials, we consider its effect. We recomputed the formation enthalpies of different phases in La–H and Y–H systems at 300 GPa by including ZPE (Fig. S5). The phases LaH_{10} and YH_{10} are still stable; therefore, the above conclusions are not altered by considering zero-point vibrations. The authors of ref. 30 focused on the YH_6 stoichiometry, and the authors did not consider hydrogen compositions higher than 1:8. To understand the role of the La atoms in stabilization of clathrate hydrogen structure, we computed the "formation volume" $V_{LaH10} - V_{H10} - V_{La}$, where V_{LaH10} is the volume of LaH_{10}, V_{H10} is the volume of hydrogen in the sodalite-like structure, and V_{La} is the volume of La at 300 GPa. We found the formation volume to be negative: -4.66 A^3 per primitive cell.

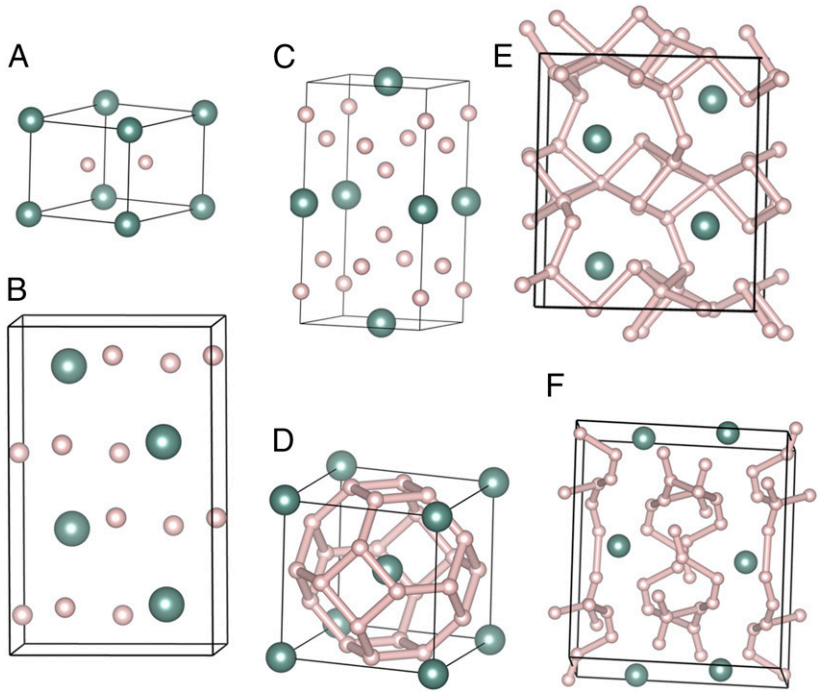

Fig. 5. Predicted yttrium hydride structures. (*A*) YH_2, (*B*) YH_3, (*C*) YH_4, (*D*) YH_6, (*E*) YH_8, and (*F*) YH_{12}. Large and small spheres represent Y and H atoms.

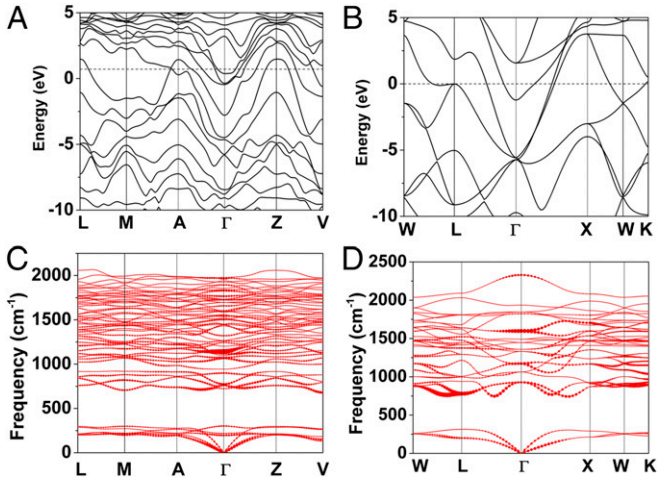

Fig. 6. Calculated electronic band structures of (*A*) LaH_8 and (*B*) LaH_{10} at 300 GPa. The phonon spectrum for (*C*) LaH_8 and (*D*) LaH_{10} at 300 GPa. Red solid circles (*Bottom*) show the EPC with the radius proportional to the respective coupling strength.

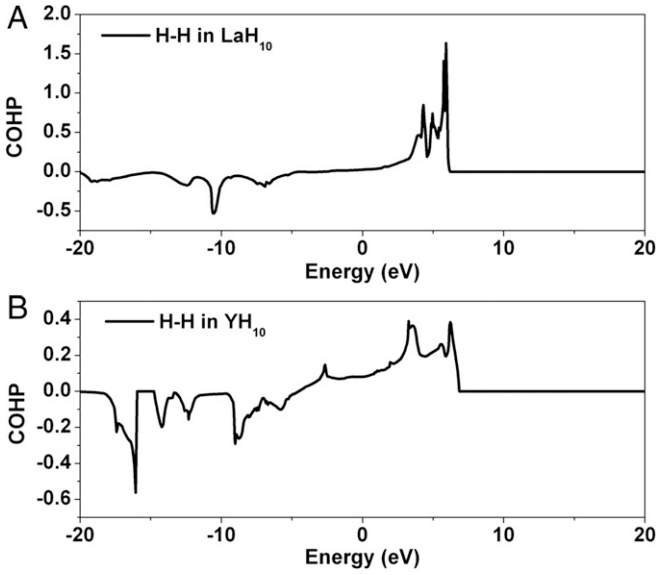

Fig. 8. COHP for pairs of H–H in (*A*) LaH_{10} and (*B*) YH_{10} at 300 GPa.

This suggests that the La atoms help to stabilize the clathrate hydrogen structure.

We also investigated the bonding in these hydrides by a crystal orbital Hamiltonian population (COHP) analysis. The COHP provides an atom-specific measure of the bonding character of states in a given energy region (47). A negative COHP indicates bonding and positive COHP indicates antibonding. As Fig. 8 shows, predictably most of the states below the Fermi level are H–H bonding for LaH_{10} and YH_{10}. The interesting difference is that some H–H antibonding states are occupied in the yttrium hydride.

We comment on the reliability of the present predictions of very high-T_c superconductivity by comparing our results with existing experimental data and additional BCS calculations for related superconductors. We calculated a T_c of 6–7 K for fcc La under ambient pressure using $\mu^* = 0.1$–0.13, which is close to previous theoretical (46) and experimental work ($T_c = 6$ K) (48), and consistent with high-pressure behavior ($T_c = 13$ K at 20 GPa) (45, 48). Likewise, our method gives the T_c of elemental Y under pressure to be 15–16 K using $\mu^* = 0.1$–0.13, which is also consistent with previous theoretical (15) and experimental studies ($T_c = 17$ K at 89 GPa) (49). All of our calculations were carried out using the harmonic approximation. It is well known that in many hydrides anharmonicity tends to lower T_c (50). For the well-studied SH_3 system, however, such an effect is weak: T_c is lowered from its harmonic 204 K value (24) only to 194 K (21) at 250 GPa, and both are close to the reported experiment T_c at that pressure (20).

There is a good reason to think that hydrogen-rich hydrides should behave similarly to pure hydrogen. Recent first-principles calculations of metallic hydrogen in structures with space groups $I4_1/amd$ and *Cmca*-4 predict anharmonic behavior that differs from calculated results for hydrides with relatively low hydrogen content (51, 52). Whereas in the $I4_1/amd$ the inclusion of anharmonicity slightly lowers T_c (i.e., from 318 to 300 K at 500 GPa), the situation is drastically different in the *Cmca-4* phase, where the calculated T_c increases by a factor of 2 with anharmonicity introduced, such that the phase is predicted to be a superconductor above 200 K. In this context it is also worth noticing that anharmonic vibrations may enhance the electron–phonon matrix elements, e.g., in the case of disordered materials (53).

In summary, exploration of La–H and Y–H systems at high pressures reveals stable hydrogen-rich phases with calculated unusually high superconducting temperatures. To be realistic, we should be careful about these high T_cs. Although well-calibrated on low T_c elemental superconductors, more high-T_c compounds need to be studied—we only have SH_3 mentioned above (with its attendant ambiguities—not in the T_c, measured, but in the structure). The predicted stabilities of the phases are in the range of current high-pressure techniques, although the megabar pressures required present challenges for combined synthesis and characterization. On the other hand, it may also be possible to synthesize these and related materials metastably at lower pressure. For instance, one might reason from the fact that Y (54) itself has a distorted fcc structure that it may be possible to produce sodalite-like YH_{10} at a metal–hydrogen interface. The exploration, theoretical and experimental, of high hydrides of heavy metals is thus a promising field (55–58).

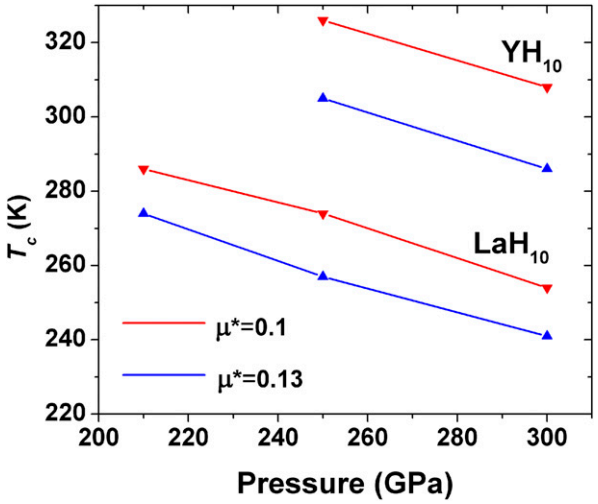

Fig. 7. Calculated T_c of LaH_{10} and YH_{10} as a function of pressure.

ACKNOWLEDGMENTS. We are grateful to the reviewers for their comments on the manuscript. This research was supported by EFree, an Energy Frontier Research Center funded by the US Department of Energy, Office of Science,

Office of Basic Energy Sciences under Award DE-SC0001057. The infrastructure and facilities used are supported by the US Department of Energy/National Nuclear Security Administration (Grant DE-NA-0002006, Capital/Department of Energy Alliance Center).

1. Ashcroft NW (1968) Metallic hydrogen: A high-temperature superconductor? *Phys Rev Lett* 21:1748.
2. Ashcroft NW (2004) Hydrogen dominant metallic alloys: High temperature superconductors? *Phys Rev Lett* 92:187002.
3. Bardeen J, Cooper LN, Schrieffer JR (1957) Microscopic theory of superconductivity. *Phys Rev* 106:162.
4. Eremets MI, Trojan IA, Medvedev SA, Tse JS, Yao Y (2008) Superconductivity in hydrogen dominant materials: Silane. *Science* 319:1506–1509.
5. Chen XJ, et al. (2008) Superconducting behavior in compressed solid SiH_4 with a layered structure. *Phys Rev Lett* 101:077002.
6. Zurek E, Hoffmann R, Ashcroft NW, Oganov AR, Lyakhov AO (2009) A little bit of lithium does a lot for hydrogen. *Proc Natl Acad Sci USA* 106:17640–17643.
7. Strobel TA, et al. (2011) High-pressure study of silane to 150 GPa. *Phys Rev B* 83: 144102.
8. Shamp A, Zurek E (2015) Superconducting high-pressure phases composed of hydrogen and iodine. *J Phys Chem Lett* 6:4067–4072.
9. Struzhkin VV, et al. (2016) Synthesis of sodium polyhydrides at high pressures. *Nat Commun* 7:12267.
10. Shamp A, Zurek E (2017) Superconductivity in hydrides doped with main group elements under pressure. *Novel Supercond Mat* 3:14–22.
11. Feng J, et al. (2006) Structures and potential superconductivity in at high pressure: En route to "metallic hydrogen". *Phys Rev Lett* 96:017006.
12. Tse JS, Yao Y, Tanaka K (2007) Novel superconductivity in metallic SnH_4 under high pressure. *Phys Rev Lett* 98:117004.
13. Gao G, et al. (2008) Superconducting high pressure phase of germane. *Phys Rev Lett* 101:107002.
14. Li Y, et al. (2010) Superconductivity at approximately 100 K in dense SiH4(H2)2 predicted by first principles. *Proc Natl Acad Sci USA* 107:15708–15711.
15. Chen Y, Hu QM, Yang R (2012) Predicted suppression of the superconducting transition of new high-pressure yttrium phases with increasing pressure from first-principles calculations. *Phys Rev Lett* 109:157004.
16. Kim DY, Scheicher RH, Ahuja R (2009) Predicted high-temperature superconducting state in the hydrogen-dense transition-metal hydride YH_3 at 40 K and 17.7 GPa. *Phys Rev Lett* 103:077002.
17. Wang H, Tse JS, Tanaka K, Iitaka T, Ma Y (2012) Superconductive sodalite-like clathrate calcium hydride at high pressures. *Proc Natl Acad Sci USA* 109:6463–6466.
18. Gao G, et al. (2013) Theoretical study of the ground-state structures and properties of niobium hydrides under pressure. *Phys Rev B* 88:184104.
19. Li Y, Hao J, Liu H, Li Y, Ma Y (2014) The metallization and superconductivity of dense hydrogen sulfide. *J Chem Phys* 140:174712.
20. Drozdov AP, Eremets MI, Troyan IA, Ksenofontov V, Shylin SI (2015) Conventional superconductivity at 203 kelvin at high pressures in the sulfur hydride system. *Nature* 525:73–76.
21. Errea I, et al. (2015) High-pressure hydrogen sulfide from first principles: A strongly anharmonic phonon-mediated superconductor. *Phys Rev Lett* 114:157004.
22. Li Y, et al. (2015) Dissociation products and structures of solid H_2S at strong compression. *Phys Rev B* 93:020103.
23. Einaga M, et al. (2016) Crystal structure of the superconducting phase of sulfur hydride. *Nat Phys* 12:835–838.
24. Duan D, et al. (2014) Pressure-induced metallization of dense $(H_2S)_2H_2$ with high-Tc superconductivity. *Sci Rep* 4:6968.
25. Drozdov AP, Eremets MI, Troyan IA (2015) Superconductivity above 100 K in PH_3 at high pressures. arXiv:1508.06224.
26. Shamp A, et al. (2016) Decomposition products of phosphine under pressure: PH_2 stable and superconducting? *J Am Chem Soc* 138:1884–1892.
27. Liu H, Li Y, Gao G, Tse JS, Naumov II (2016) Crystal structure and superconductivity of PH_3 at high pressures. *J Phys Chem C* 120:3458–3461.
28. Flores-Livas JA, et al. (2016) Superconductivity in metastable phases of phosphorus-hydride compounds under high pressure. *Phys Rev B* 93:020508.
29. Feng X, Zhang J, Gao G, Liu H, Wang H (2015) Compressed sodalite-like MgH_6 as a potential high-temperature superconductor. *RSC Adv* 5:59292–59296.
30. Li Y, et al. (2015) Pressure-stabilized superconductive yttrium hydrides. *Sci Rep* 5:9948.
31. Wang Y, Lv J, Zhu L, Ma Y (2010) Crystal structure prediction via particle-swarm optimization. *Phys Rev B* 82:094116.
32. Wang Y, Lv J, Zhu L, Ma Y (2012) CALYPSO: A method for crystal structure prediction. *Comput Phys Commun* 183:2063–2070.
33. Liu H, Wang H, Ma Y (2012) Quasi-molecular and atomic phases of dense solid hydrogen. *J Phys Chem C* 116:9221–9226.
34. Zhu L, et al. (2011) Substitutional alloy of Bi and Te at high pressure. *Phys Rev Lett* 106:145501.
35. Zhang M, et al. (2015) Two-dimensional boron-nitrogen-carbon monolayers with tunable direct band gaps. *Nanoscale* 7:12023–12029.
36. Miao MS (2013) Caesium in high oxidation states and as a p-block element. *Nat Chem* 5:846–852.
37. Zhu L, Liu H, Pickard CJ, Zou G, Ma Y (2014) Reactions of xenon with iron and nickel are predicted in the Earth's inner core. *Nat Chem* 6:644–648.
38. Yong X, et al. (2016) Crystal structures and dynamical properties of dense CO_2. *Proc Natl Acad Sci USA* 113:11110–11115.
39. Liu H, Naumov II, Hemley RJ (2016) Dense hydrocarbon structures at megabar pressures. *J Phys Chem Lett* 7:4218–4222.
40. Perdew JP, Burke K, Ernzerhof M (1996) Generalized gradient approximation made simple. *Phys Rev Lett* 77:3865–3868.
41. Amri M, Clarkson GJ, Walton RI (2010) Anisotropic thermal expansion of SiO_2 and $AlPO_4$ clathrasils with the AST-type structure. *J Phys Chem C* 114:6726–6733.
42. Papaconstantopoulos D, Klein B, Mehl M, Pickett W (2015) Cubic H_3S around 200 GPa: An atomic hydrogen superconductor stabilized by sulfur. *Phys Rev B* 91:184511.
43. McMahon JM, Ceperley DM (2011) Ground-state structures of atomic metallic hydrogen. *Phys Rev Lett* 106:165302.
44. Dynes R (1972) McMillan's equation and the T_c of superconductors. *Solid State Commun* 10:615–618.
45. Nixon LW, Papaconstantopoulos DA, Mehl MJ (2008) Electronic structure and superconducting properties of lanthanum. *Phys Rev B* 78:214510.
46. Bağci S, Tutuncu H, Duman S, Srivastava G (2010) Phonons and superconductivity in fcc and dhcp lanthanum. *Phys Rev B* 81:144507.
47. Dronskowski R, Bloechl PE (1993) Crystal Orbital Hamilton Populations (COHP). Energy-resolved visualization of chemical bonding in solids based on density-functional calculations. *J Phys Chem* 97:8617–8624.
48. Tissen VG, Ponyatovskii EG, Nefedova MV, Porsch F, Holzapfel WB (1996) Effect of pressure on the superconducting T_c of lanthanum. *Phys Rev B: Condens Matter* 53: 8238–8240.
49. Hamlin J, Tissen V, Schilling J (2006) Superconductivity at 17 K in yttrium metal under nearly hydrostatic pressures up to 89 GPa. *Phys Rev B* 73:094522.
50. Errea I (2016) Approaching the strongly anharmonic limit with ab initio calculations of materials—Vibrational properties colloquium. *Eur Phys J B* 89:237.
51. Borinaga M, et al. (2016) Anharmonic enhancement of superconductivity in metallic molecular Cmca-4 hydrogen at high pressure: A first-principles study. *J Phys: Condens Matter* 28:494001.
52. Borinaga M, Errea I, Calandra M, Mauri F, Bergara A (2016) Anharmonic effects in atomic hydrogen: Superconductivity and lattice dynamical stability. *Phys Rev B* 93: 174308.
53. Garland J, Bennemann K, Mueller F (1968) Effect of lattice disorder on the superconducting transition temperature. *Phys Rev Lett* 21:1315.
54. Samudrala GK, Tsoi GM, Vohra YK (2012) Structural phase transitions in yttrium under ultrahigh pressures. *J Phys Condens Matter* 24:362201.
55. Zaleski-Ejgierd P, Labet V, Strobel TA, Hoffmann R, Ashcroft NW (2012) WH(n) under pressure. *J Phys: Condens Matter* 24:155701.
56. Zaleski-Ejgierd P, Hoffmann R, Ashcroft NW (2011) High pressure stabilization and emergent forms of PbH_4. *Phys Rev Lett* 107:037002.
57. Zhong X, et al. (2016) Tellurium hydrides at high pressures: High-temperature superconductors. *Phys Rev Lett* 116:057002.
58. Kim DY, Scheicher RH, Pickard CJ, Needs RJ, Ahuja R (2011) Predicted formation of superconducting platinum-hydride crystals under pressure in the presence of molecular hydrogen. *Phys Rev Lett* 107:117002.